ELSEVIER

Earth and Planetary Science Letters 203 (2002) 45–57

EPSL

www.elsevier.com/locate/epsl

Where did rotational shortening occur in the Himalayas? – Inferences from palaeomagnetic remagnetisations

E. Schill [a,b,*], C. Crouzet [a], P. Gautam [a,c], V.K. Singh [d], E. Appel [a]

[a] Institut für Geologie, Universität Tübingen, Sigwartstraße 10, 72076 Tübingen, Germany
[b] Institut für Geophysik, ETH Zürich, Hönggerberg HPP O14, 8093 Zürich, Switzerland
[c] Central Department of Geology, Tribhuvan University, Kirtipur, Kathmandu, Nepal
[d] Department of Geology, Bundelkhand University, Jhansi 284128 U.P., India

Received 17 January 2002; received in revised form 8 July 2002; accepted 10 July 2002

Abstract

In metacarbonates of the Lesser (LH) and Tethyan (TH) Himalayas of Kumaon/Garhwal (N-India) characteristic remanent magnetisations carried by pyrrhotite (unblocking temperatures: 250–330°C) and magnetite (demagnetising spectra: 15–50 mT) have been identified. Negative fold tests indicate remanence acquisition after the main folding phase, which is of short-wavelength character and occurs during the early orogenese of the Himalayas. A thermal or thermochemical origin of magnetisation is likely and the age of remanence acquisition is indicated to be about 40 Ma by $^{40}K/^{39}Ar$ cooling and $^{40}Ar/^{39}Ar$ crystallisation ages. In the Kumaon LH a long-wavelength tilting is indicated by a distribution of the remanence directions along a small-circle in N–S direction. Steepening of the remanence directions in the TH related to ramping on the Main Central Thrust (MCT) was not observed, in contrast to other related studies. In the Alaknanda valley of LH a 38 ± 8 Ma age of remanence acquisition is supported by comparison of observed inclinations to the apparent polar wander path of India. Clockwise rotation of $20.3 \pm 11.7°$ (LH/Alaknanda valley) and $11.3 \pm 8.5°$ (TH) with respect to the Indian plate is observed, indicating that there is no significant evidence for rotational shortening along the MCT since about 40 Ma. Our results suggest that most of rotational underthrusting and oroclinal bending has not been accommodated by the MCT, but by the main thrusts south of it. The latest Miocene/Pliocene age of the Main Boundary Thrust indicates that oroclinal bending is a late-orogenic process.

Keywords: paleomagnetism; Himalayas; rotation; crustal shortening; secondary magnetization; remanent magnetization

1. Introduction

The Early Tertiary India–Asia collision and related shortening of the colliding margins resulted in the formation of the Himalayan Orogen. In the context of the movement of the Indian plate and relative movements between the Indian shield and its northern margin, the total shortening can be subdivided into ‘straight forward’ shortening in an approximately north–south direction and rotational shortening. The rotational shortening represents the sum of rotational underthrusting of India beneath the northern Indian margin and

* Corresponding author. Tel.: +41-1-6333667; Fax: +41-1-6331065.
E-mail address: schill@mag.ig.erdw.ethz.ch (E. Schill).

0012-821X/02/$ – see front matter
PII: S0012-821X(02)00842-7

Asia due to the counterclockwise rotation of India plus the shortening caused by the bending of the Himalayan belt due to the overthrusting of the northern Indian margin onto the Indian shield. Oroclinal bending can be described by a series of block rotations around individual pivots as a consequence of rotational underthrusting as suggested by [1] or by continuous bending by crustal downwarp of the Indian shield in the broader framework of a small-circle tracing the Himalayan Arc around the so-called Turfan pole as suggested by [2,3]. Its controlling mechanism is assumed to be the pinning of the rotation of the Indian shield in the NW-Himalayan Syntaxis and the underthrusting of the Indian lithosphere along the Main Central Thrust (MCT) and the successively southward propagating younger thrusts [1]. Rotational underthrusting can be regarded as driven by a uniform counterclockwise movement of the Indian shield around a pivot in the NW Syntaxis (35°N, 73°E) [2], causing the relative movement between the Indian shield and its northern continental margin. Palaeomagnetic results from the Tethyan Himalaya have been used to detect and quantify such rotations with respect to the Indian shield [2,4–9]. In low-grade metacarbonates of the Tethyan and Lesser Himalayas, along the Himalayan Arc, secondary thermoremanent (TRMs), partial TRMs, or thermochemical magnetisations carried by pyrrhotite are frequently observed and interpreted in terms of tilting and rotations [5–8,10,11]. Remanence inclinations that are $\sim$20° steeper than expected from the Indian apparent polar wander path (APWP) in the Tethyan sediments of Manang area (central Nepal) have been related to ramping along the MCT [5]. Oversteepened inclinations were also reported from the pyrrhotite component of the Everest leucogranite ($\sim$10° steeper than expected) [12] and from metacarbonates in the Thakkhola area and Hidden Valley (western Nepal; $\sim$20–25° steeper than expected) [4,8]. In the Shiar Khola area (central Nepal) varying inclinations are interpreted in terms of N–S directed long-wavelength folding after remanence acquisition [11].

In the Garhwal Himalaya clockwise rotations of $\sim$25° with respect to the Indian shield since 30–20 Ma were concluded from remanences with unblocking temperatures of 270–330°C in the Krol Belt sequence of the Lesser Himalaya (sites k1–k6; Fig. 1) [9]. From the results of the Alaknanda valley (sites al1–al8; Fig. 1) [10] clockwise rotations of $\sim$30–20° can be concluded for assumed magnetisation ages in the range of 40–10 Ma (corresponding to cooling ages of the area [16]). It has been shown that regional block rotations ought to be scrutinised for possible local effects in order to minimise erroneous estimates of rotational shortening caused by the rotation of India [6]. Rotations close to the Syntaxis appear to be dominated by local tectonics, while the record of regional dynamics becomes more important with increasing distance [7]. Systematic combination of palaeomagnetic results and structural information has been used to calculate a uniform total rotational shortening between the Indian shield and its northern margin in the western Himalaya [7]. Former studies dealt with the overall relative rotation between the Indian shield and its northern margin (represented by the Tethyan Himalaya). In our study we focus on rotations on a NW–SE profile across the strike of the Himalayan Arc from south of the MCT to an area directly north of the Malari (detachment) fault (Fig. 1). Among the thrusts at the base of the High Himalayan Crystalline (HHC) and further to the south, the MCT has accommodated the highest amount of 'straight forward' shortening, estimated between several tens of kilometers to 150–250 km [17]. The shortening along the Main Boundary Thrust (MBT) is generally estimated to be several tens of kilometers, but much larger shortening has been suggested ([17] and references therein). Our data provide information on possible rotational shortening along the MCT, assesses where the rotational movement is distributed across the Himalayan thrust and contributes to the interpretation of the observed oversteepened remanence inclinations.

2. Geology of the sampled areas

The MCT separating the HHC from the Lesser Himalaya metasediments appears to be the most prominent of the southward propagating thrusts.

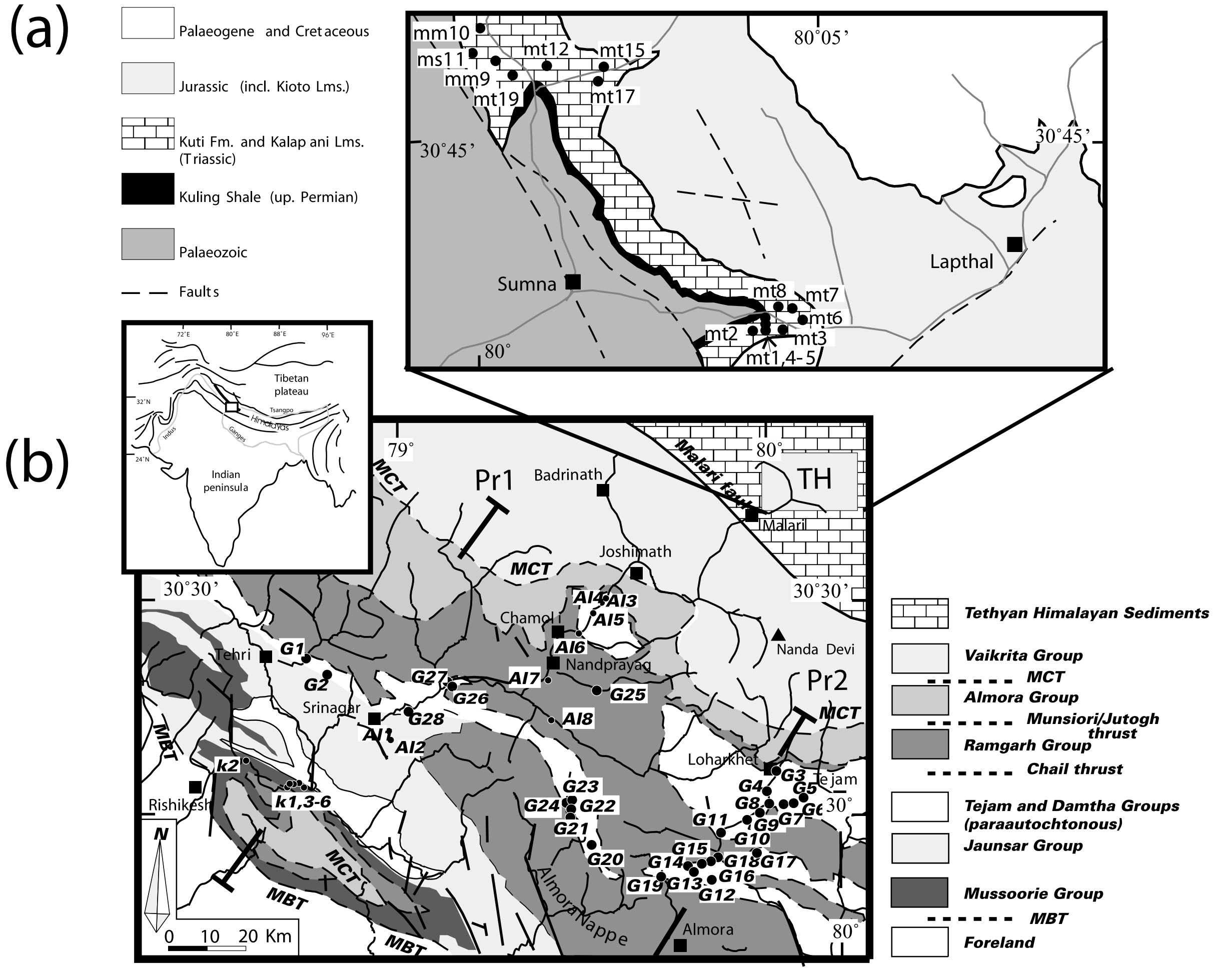

Fig. 1. Geological maps of the Kumaon/Garhwal area. The open rectangle in the small figure marks the geographic position of the area. (a) Geological map of the Kumaon Tethyan Himalayas after [13] with site locations for this study (mt1–8, 12, 15, 17, 19, mm9, 10, ms11). (b) Geological map of Lesser Kumaon Himalayas (modified after [14]) with the site locations for this study (sites g1–28) and also for [9] (sites k1–6) and [10] (sites al1–8). MBT: Main Boundary Thrust; MCT: Main Central Thrust; TH: sampling area in the Kumaon Tethyan Himalayas. The profiles Pr1 and Pr2 simplified from [15] are shown in Fig. 7.

In order to study relative rotations along this thrust, low-grade metamorphic carbonates to the south of the MCT were sampled in the Lesser Kumaon/Garhwal Himalaya (LH samples, SSW of the Nanda Devi Massif; Fig. 1b). Due to absence of metacarbonates in the HHC they were sampled from the Tethyan Himalaya of Malari area (TH samples; Fig. 1a) north of the Malari Fault (probably part of the South Tibetan Detachment Fault System, STDS). The thermal evolution of the Higher Himalaya is characterised by two metamorphic phases: a collision-related Eohimalayan phase (40–35 Ma) and a Neohimalayan phase (22–18 Ma) [18,19]. In both areas low-grade metamorphic carbonates of various formations were sampled. The Lesser Himalaya (metasediments of mainly Precambrian to Early Palaeozoic age) overthrusts the Siwalik molasse basin to the south along the MBT and is itself overthrusted by the HHC along the MCT. The Lesser Himalaya is extensively folded and faulted [13]. Four folding phases were recognised in the Kumaon/Garhwal Himalayas. The two older phases with structures trending generally E–W to NW–SE are related to the Eohimalayan orogenesis, while the fold axes of the younger phases trend N–S to NE–SW. The youngest phase developed under brittle condition [20]. The eastern part of the sampling area is dominated by the influence of the Almora nappe, which is part of the High Himalayan sequence. Detailed structural and geochronological studies from its eastward continuation, the Dadeldhura nappe, and the underlying Lesser Himalaya of far western Nepal indicate an emplacement of the Dadeldhura thrust sheet at 22–15 Ma and the growth of a Lesser Himalayan duplex between 12 and 5 Ma [21]. Two profiles across the sampling area show the general geological structures and the differences in the duplex structures (see below) in the NW and SE of the LH sampling areas [15]. The North of the HHC and the Tethyan Sedimentary Series (diagenesis–anchizonal metasediments of Precambrian to Eocene age) are detached along the Malari Fault, which may be related to the STDS. NW–SE striking fold axes are dominant in the Tethyan Himalaya [13].

South of the MCT in the LH area 28 sites (g1–g28) were sampled in epizonal metacarbonates of the Tejam and Damtha Groups (Late Palaeoproterozoic age [22]; Fig. 1). In the TH area, 12 sites were sampled from the Lower Triassic Kalapani Limestone and a further three sites from the Middle Triassic Kuti Formation (Fig. 1).

3. Sample treatment and measurements

A portable rockdrill was used for sampling. Cores were oriented with a magnetic compass. Due to the low intensity, orientation with a solar compass is not required. In general, about 10 cores, 2.5 cm in diameter, were taken at each site.

The cores were sliced into specimens of standard length (2.2 cm). All magnetic measurements were carried out in the palaeomagnetic laboratory of the University of Tübingen (Germany). The natural remanent magnetisation (NRM) of two pilot specimens was progressively demagnetised, for one specimen by heating in a MMTD1 furnace (Magnetic Measurements), for the other by alternating fields (AF) treatment using an automatic degaussing system (2G Enterprises 2G600). Remanence directions and intensities were measured with a 755R SQUID magnetometer (2G Enterprises; noise level <0.01 mA m^{-1} for 10 cm^3 specimens). Low-field magnetic susceptibility was monitored after each heating step to detect possible changes in magnetic mineralogy. The anisotropy of low-field magnetic susceptibility (AMS; for all samples) and anisotropy of anhysteretic remanence (AARM; for selected sites) was measured to check for a possible deviation of the remanence direction. For selected samples anisotropy in the saturation magnetisation has been investigated using a torque meter at the ETH Zürich (Switzerland) [23]. The AF-demagnetised specimens were subsequently used for isothermal remanence (IRM) acquisition with a MMPM9 pulse magnetiser (Magnetic Measurements) with a maximum field of 2.75 T followed by stepwise thermal demagnetisation of the saturation IRM (SIRM). The intensity of IRM was measured with a Minispin spinner magnetometer (Molspin; noise level about 0.2 mA m^{-1} for 10 cm^3 specimens). Following the pilot results the remaining specimens were first heated up to 150°C to destroy a possible goethite component. The specimens of LH were further demagnetised either thermally in steps of 50–5°C, by suitable AF steps or by a combination of both. The specimens of TH were demagnetised in an alternating field using 2–20mT steps up to 140 mT. Specimens with a residual intensity $>10\%$ of the initial magnetisation were subsequently further demagnetised in 20°C steps from 250 to 350°C. Despite of working in a low magnetic field environment, between each thermal demagnetisation step and the remanence measurement the specimens were also subjected to AF treatment at 20 mT in order to remove possible viscous magnetisation acquired by the very soft magnetite fraction. Orthogonal vector projections, equal area projections and principal component analysis (PCA) were used for determination of remanence components. For the determination of rotations around vertical axes the angle between observed and expected remanence directions from the APWP for the respective ages are used for Fisher distributed site mean directions. The direction defined by the intersection of the small-circle, representing the distribution of site mean directions, and the small-circle of common inclination through the expected remanence direction (from the APWP) is used for small-circle distributed site mean directions following the method of [24].

4. Magnetic mineralogy and palaeomagnetic results

Alternating field as well as thermal demagnetisation was used to separate three significant remanence components (apart from goethite), composing the NRM of the metacarbonates of both areas, according to their unblocking spectra (Figs. 2 and 3). These three components are:

1. In the TH area only, a low-coercive magnetite (demagnetised below 10 mT; Fig. 3), carrying an in situ remanence direction close to the local present field (mean $D/I = 358°/42°$, $\alpha_{95} = 5.3°$, $k = 68.8$, $N_{sites} = 12$; ambient field $D/I = 1°/46°$);
2. A high-coercive magnetite component (demagnetised between 25 and 70 mT; Fig. 3), which carries a characteristic remanent magnetisation ($ChRM_{MAG}$) in the TH area. A well-grouped overall mean direction in geographic coordinates could be obtained for this magnetite component for site mean results with $k > 10$ (mean $D/I = 7.5°/26.6°$, $\alpha_{95} = 7.6°$, $k = 41.4$, $N_{sites} = 10$; Fig. 4a and Table 1). In the LH area, five of 28 sites show well-defined groupings within each site, but the site mean directions are randomly distributed and not useful for further interpretation in terms of rotations;
3. In both areas pyrrhotite has been identified by its unblocking temperature spectrum (250–330°C; Figs. 2 and 3). In 20 of 28 sites from the LH area, pyrrhotite is the main remanence carrier ($ChRM_{PYR}$). Directional analyses were carried out using linear PCA of the thermal demagnetisation data in Zijderveld plots (in the unblocking range of 275–330°C) as well as stable endpoint directions of the residual magnetic component after AF demagnetisation up to 140 mT. In several sites two antiparallel components carried by pyrrhotite were observed during thermal demagnetisation, possibly representing a pTRM reversal record [8]. Well-grouped ($k \geq 10$) specimen directions have been obtained for 18 sites (Table 2). In

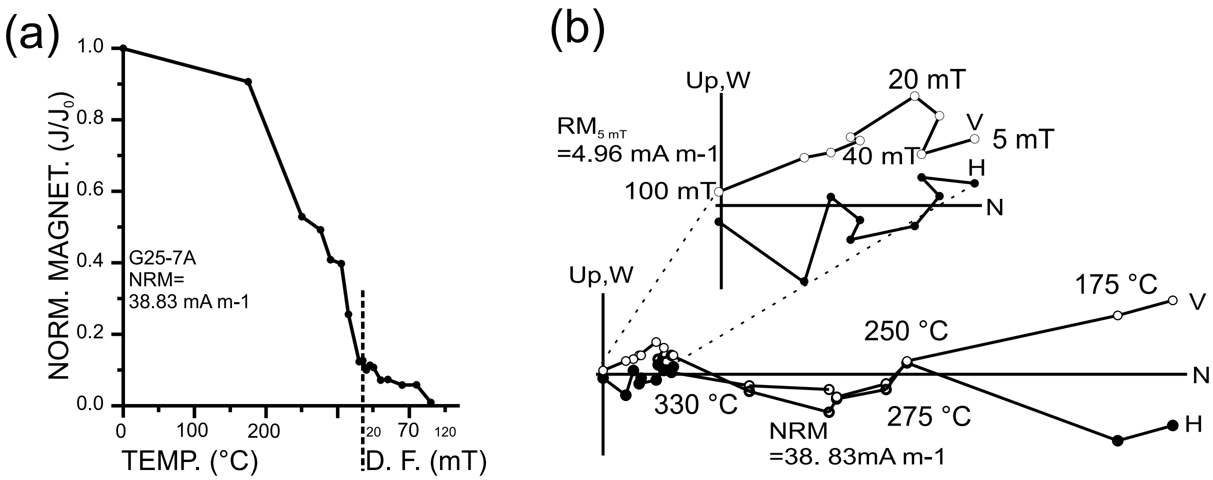

Fig. 2. Thermal and alternating field (AF) demagnetisation of a representative sample from the LH area in geographic coordinates. (a) Intensity plot of combined thermal and subsequent AF demagnetisation of the natural remanent magnetisation (NRM). (TEMP.: temperature; D.F.: demagnetising field), showing a pyrrhotite component and minor magnetite content. (b) Orthogonal vector projection of the combined thermal and AF demagnetisation. Zoom: Orthogonal vector projection of the AF demagnetisation ($RM_{5\,mT}$: remanent magnetisation after the 5 mT demagnetising step; V (open circles): vertical projection; H (full circles): horizontal projection).

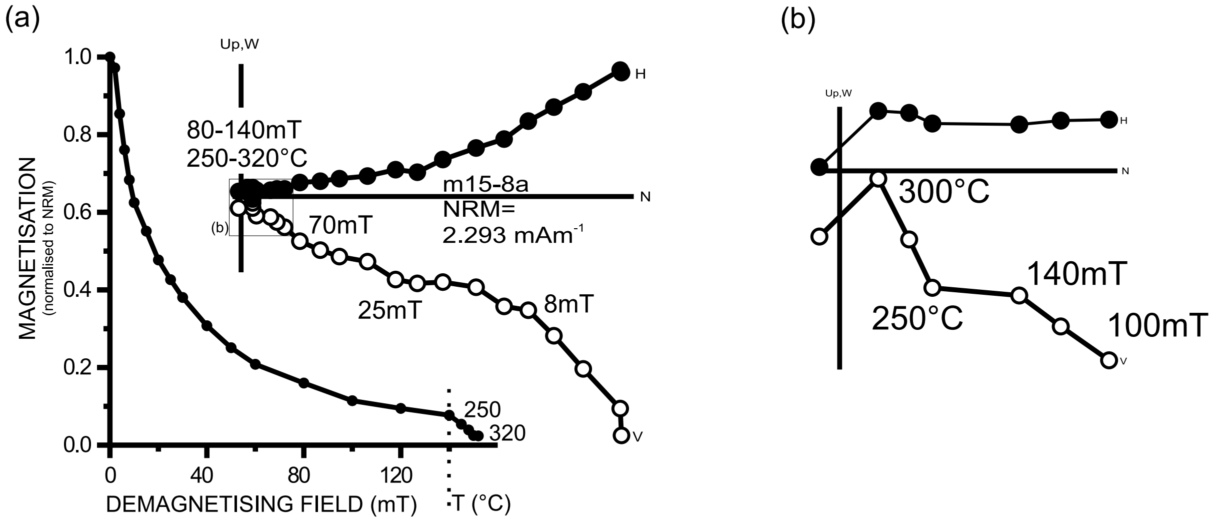

Fig. 3. AF and subsequent thermal demagnetisation of a representative sample of the sampling area TH in geographic coordinates after breakdown of goethite at 150°C with orthogonal vector projection of the AF demagnetisation (a) and thermal demagnetisation (b). T: temperature, see caption to Fig. 2.

the Kalapani Limestone of the TH area only, a third residual component (generally demagnetised above 80 mT) is observed after AF demagnetisation. The high coercivity of this ChRM indicates pyrrhotite ($ChRM_{PYR}$) as the remanence carrier and this is confirmed subsequently by thermal demagnetisation of several specimens (unblocking temperature range of 250–300°C; Fig. 3). Linear and planar PCA were used to analyse pyrrhotite as the remanence carrier of the residual component, resulting in concurrent in situ mean directions determined by AF demagnetisation (mean of $ChRM_{PYR}$: $D/I = 7.6°/34.0°$, $\alpha_{95} = 13.4°$, $k = 13.9$, $N_{sites} = 10$; Fig. 4b and Table 3) using site means with $k > 10$ and by thermal demagnetisation (mean of $ChRM_{PYR}$: $D/I = 6.7°/32.2°$, $\alpha_{95} = 14.6°$, $k = 10.7$, $N_{specimens} = 11$; Fig. 4b).

4.1. Discussion of the palaeomagnetic results

Anisotropy of remanence carriers may influence the remanence direction significantly. Indeed, the AMS measurements reveal a high degree of anisotropy ($P' \geq 1.2$) for five sites in the LH area (Table 2). Generally, magnetic susceptibility measurements are dominated by the magnetite fraction and pyrrhotite has only a minor contribution to the signal. Such a high degree of anisotropy can be attributed to minerals with high crystalline anisotropy such as pyrrhotite, but alternatively in the other samples a high crystalline anisotropy of pyrrhotite cannot be excluded. However, AMS as well as AARM measurements do not reveal comprehensive information on the origin of the anisotropy due to the contribution of paramagnetic and ferrimagnetic phases or of different ferrimagnetic components to the susceptibility signal and neither do AARM measurements. High field torque magnetometer measurements provide information about anisotropy in the saturation magnetisation of the ferrimagnetic content. It is possible to distinguish between different directions of the magnetite and the pyrrhotite components. In selected specimens, however, low torque impeded the determination of the ferrimagnetic anisotropy tensor. A possible influence of anisotropy on remanence directions therefore must be regarded as undeterminable in this case. All site mean directions with $k > 10$ are included in the statistics.

In the TH area, both magnetite and pyrrhotite display comparable remanence directions (Fig. 4). A fold test for the magnetite component indicates a post-folding origin on a 95% significance level

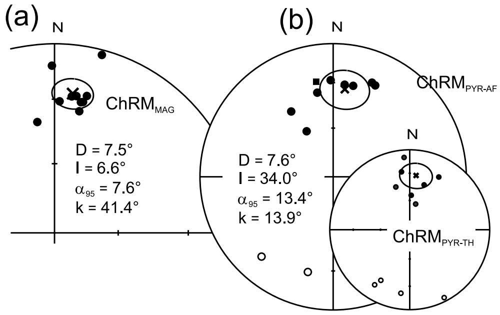

Fig. 4. Equal-area projection of site mean directions with their overall mean (×) and α_{95} angles for ChRM$_{MAG}$ (a) and ChRM$_{PYR}$ (b) of area TH in geographic coordinates, both plotted in the lower hemisphere (open/full circles: site mean directions plotted in the upper/lower hemisphere). The small stereo plot of (b) shows single specimen directions of several sites obtained by thermal demagnetisation (TH) after AF treatment and their mean direction (×) plotted in the lower hemisphere.

(with critical limit of χ ratio = 3.497) with χ_{str}/χ_{geo} = 3.923 (after [25]) and partial unfolding shows best grouping at −21% unfolding. A fold test of the pyrrhotite component is statistically insignificant and partial unfolding shows ambiguous results. The low significance level of the fold tests results from comparable bedding attitudes for most of the sites (Tables 1 and 3).

In the LH area a pyrrhotite component has previously been identified in the Garhwal Himalaya [10]. These previous results are included in the present statistical analyses as well as results for component B [9] (Late Tertiary secondary component, post-folding), which we believe is also carried by pyrrhotite according to the unblocking temperatures of 270–330°C. A negative fold test for site g17 and for the site mean directions (with critical limit of χ ratio = 6.371) with χ_{str}/χ_{geo} = 7.818 (95% after [25]) indicates remanence acquisition after the main folding of the Himalayas. Partial unfolding shows best grouping at 15% of unfolding and confirms a post-folding origin, which we interpret as remanence acquisition in the final stage of the main Himalayan deformation.

It is obvious that the distribution of site mean directions in the LH area is different for the

Table 1
Statistical parameters for the ChRM$_{MAG}$ of the TH area

Site	Geographic position		N/M	Geographic coordinates				Bedding	
	N (°)	E (°)		Dec.	Inc.	α_{95}	k	Dip dir.	Dip
mt1	30.7267	80.0772	10/10	**9.1**	**27.6**	17.0	10.1	45.0	32.0
mt2	30.7248	80.0765	10/11	**11.4**	**30.2**	6.9	50.4	45.0	32.0
mt3	30.7267	80.0833	11/11	**12.3**	**29.9**	11.9	15.6	63.0	31.0
mt4	30.7218	80.0748	11/11	**11.5**	**34.7**	7.2	46.2	30.0	30.0
mt5	30.7210	80.0755	6/6	**13.3**	**26.5**	9.8	47.9	30.0	30.0
mt6	30.7320	80.0800	10/10	**2.2**	**31.0**	9.9	24.8	60.0	25.0
mt7	30.7313	80.0783	9/9	**7.2**	**28.1**	6.1	71.4	60.0	28.0
mt8	30.7307	80.0765	9/9	19.7	18.6	22.1	7.2	65.0	33.0
mm9	30.7897	80.0090	9/10	**14.9**	**3.0**	12.1	19.1	357.0–13.0	18.0–23.0
mm10	30.8018	80.0017	9/11	329.0	−24.3	25.7	5.0	34.0	67.0
ms11	30.7830	79.9977	7/8	11.3	−44.5	24.2	8.6	283.0	29.0
mt12	30.7858	80.0220	10/10	357.9	−28.9	38.1	2.6	25.0	15.0
mt15	30.7878	80.0343	7/10	**359.1**	**12.6**	17.3	13.1	8.0	11.0
mt17	30.7830	80.0327	8/9	7.4	7.4	22.8	6.8	13.0	14.0
mt19	30.7830	80.0097	7/9	**351.2**	**40.4**	11.6	27.9	105.0	13.0
Mean 10 sites ($k > 10$)				Geographic coordinates					
				7.5	**26.6**	**7.6**	**41.4**		
				Stratigraphic coordinates					
				12.6	**6.9**	**10.3**	**23.1**		

N, E: geographic latitude and longitude; N/M: number of specimens included in the statistics/measured; Dec.: declination; Inc.: inclination; α_{95}: 95% confidence angle; k: precision parameter; Dip (dir.): dip (direction) of beds; mt: Kalapani limestones; mm and ms: Kuti Formation. Only site mean values with $k > 10$ (in bold) are included in the statistics.

Table 2
Statistical parameters for the $ChRM_{PYR}$ of the area LH (explanation, see Table 1)

Site	Geographic position		N/M	AF/TH/ AF+TH	Geographic coordinates				Bedding		D. Aniso.
	N (°)	E (°)			Dec.	Inc.	α_{95}	k	Dip dir.	Dip	P'
g1	30.080	78.785	4/11	5/2/4	11.4	7.5	66.2	2.9	263.0	47.0	1.024
g2	30.062	78.844	5/10	5/2/3	**72.7**	**64.3**	14.4	29.0	300.0	20.0	1.015
g3	30.239	79.892	0/11	9/2/0	remanence intensity too low						
g4	30.179	79.886	4/11	1/9/1	4.6	−27.7	11.9	60.7	250.0	82.0	1.251
g5	30.197	79.971	6/13	1/12/0	61.9	−9.0	14.5	22.3	140.0	28.0	1.311
g6	30.171	79.955	6/6	1/5/0	**171.9**	**−3.8**	14.1	30.5	133.0	26.0	1.012
g7	30.161	79.935	0/11	9/2/0	remanence intensity too low						
g8	30.150	79.904	0/10	8/2/0	no pyrrhotite content						
g9	30.117	79.892	0/6	1/0/5	no stable directions						
g10	30.088	79.870	0/11	1/10/0	remanence intensity too low						
g11	30.033	79.825	7/7	5/1/1	**172.9**	**38.5**	23.6	11.5	205.0	48.0	1.055
g12	29.906	79.843	6/12	1/10/2	344.5	24.4	29.3	6.2	10.0	46.0	1.245
g13	29.911	79.798	9/12	1/11/0	**6.7**	**−5.0**	7.9	43.2	37.0	28.0	1.009
g14	29.922	79.782	5/11	9/2/0	166.2	−32.7	35.8	5.5	14.0	37.0	1.041
g15	29.937	79.809	5/11	1/10/1	**343.6**	**13.6**	19.3	16.6	83.0	45.0	1.027
g16	29.950	79.825	0/10	2/7/1	NRM dominated by hematite						
g17	30.015	79.917	7/14	2/11/1	**6.8**	**40.0**	8.2	55.6	130.0–350.0	12.0–78.0	1.042
g18	29.968	79.836	0/12	6/6/0	NRM dominated by hematite						
g19	29.870	79.728	8/12	7/2/3	**345.9**	**13.0**	14.8	11.7	343.0	47.0	1.046
g20	29.885	79.557	5/10	6/3/1	**358.5**	**0.5**	26.0	13.4	93.0	50.0	1.038
g21	29.935	79.485	10/12	1/11/0	52.4	4.7	11.7	17.9	110.0	34.0	1.355
g22	29.955	79.481	4/9	7/2/1	**21.0**	**29.2**	19.8	80.6	195.0	58.0	1.026
g23	29.976	79.474	9/12	9/0/0	**4.6**	**64.2**	7.0	56.4	37.0	44.0	1.013
g24	29.966	79.467	10/12	1/11/0	15.8	45.4	5.2	86.4	210.0	70.0	1.187
g25	30.270	79.440	8/14	1/10/4	358.1	−11.1	14.6	13.4	247.0	51.0	3.120
g26	30.145	79.125	9/10	6/2/2	**167.9**	**-27.2**	17.7	17.2	75.0	27.0	1.011
g27	30.153	79.112	7/8	7/1/0	**176.7**	**−25.9**	14.6	22.1	90.0	15.0	1.014
g28	30.046	79.053	7/8	4/1/3	**195.6**	**5.5**	22.6	12.4	160.0	45.0	1.013
al2*			5		206.8	4.0	15.7	26.2	185.0	66.0	
al3*			9		193.2	−35.1	7.2	51.9	119.0	18.0	
al4*			10		208.8	−22.2	9.1	29.0	43.0	23.0	
al5*			11		204.0	−17.8	10.1	21.3	135.0	11.0	
al7*			4		210.0	−24.7	31.8	10.3	95.0	42.0	
al8*			6		183.0	−42.3	12.8	39.2	328.0	31.0	
Mean 13+6*+7** sites ($k > 10$)					Geographic coordinates						
					191.0	**−26.3**	**10.0**	**9.0**			
Mean 13+6*+7** sites ($k > 10$)					Stratigraphic coordinates						
					187.6	**−33.0**	**15.2**	**4.5**			

AF: number of specimens demagnetised by alternating field; TH: number of specimens demagnetised thermally; AF+TH: number of specimens demagnetised thermally and in alternating field; P': degree of anisotropy; *[9]; **[10]. Mean directions marked in bold are included in the statistical mean.

northwestern part (Alaknanda valley; Fig. 5a) and for the southeastern part (Kumaon LH, Fig. 5b). Whereas the sites from the Alaknanda valley (g2, g25–28 (this study), al1–al8 [10], k1–k6 [9]) show well-grouped site mean directions with $k = 12.0$ and an overall in situ mean direction of $D = 196.8°/I = -29.7°$ ($\alpha_{95} = 10.4$, $N = 19$; Fig. 5a), remanence directions in the southeastern area (g4–6, g11, g13, g15, g17, g19–24) seem more likely to be distributed along a small-circle in an approximately north–south direction (Fig. 5b,c). An optimum small-circle with the pole ($D = 87°/$

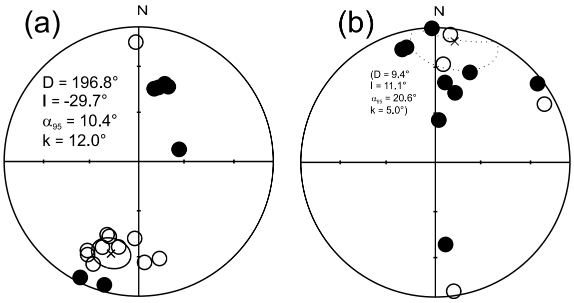

Fig. 5. (a) Site mean directions with their overall mean (×, plotted in the upper hemisphere) and α_{95} angles for $ChRM_{PYR}$ of the Alaknanda valley in geographic coordinates (LH; sites: g2, g25–28 (this study), al1–8 [10], k1–6 [9]) plotted in the upper hemisphere (open/full circles: site mean directions plotted in the upper/lower hemisphere). (b) As above, with overall mean (×, plotted in the lower hemisphere) for $ChRM_{PYR}$ of the Kumaon LH area (sites: g4–6, g11, g13, g15, g17, g19–24).

$I = -4°$) and an opening angle $\beta = 86°$ (with a standard deviation $d = 6.7°$ and α_{95} confidence angle of 4.4°) has been obtained with forward modelling with least-squares fitting using the shortest distance between the data and given small-circles over the whole sphere in 2° steps [11], excluding the two outliers (sites g5 and g21; Fig. 6a).

5. Tectonic interpretation

5.1. Origin of pyrrhotite and age of magnetisation

In marly carbonates pyrrhotite can be formed at elevated temperatures during low-grade metamorphism [27,28]. Amongst other processes pyrrhotite can be formed from sedimentary magnetite and pyrite [29]. This transformation may occur at temperatures of about $\geq 200°C$ [30], relating the process of remanence acquisition to metamorphism. A negative fold test would indicate remanence acquisition after the main deformation. The amount of newly formed pyrrhotite is a function of the thermal condition [11]. In samples with a thermoremanent magnetisation (TRM with peak metamorphic temperature $> 325°C$) the ChRM is carried by pyrrhotite, whereas at blocking temperatures $< 325°C$ the contribution of magnetite increases with decreasing temperature. In the TH area the low contribution of pyrrhotite to the total NRM is an indicator for low temperatures (distinctly lower than 325°C) during metamorphism and a thermochemical remanent magnetisation of pyrrhotite is likely. The age of remanence acquisition in the TH area can be related to $^{40}Ar/$

Table 3
Statistical parameters for the $ChRM_{PYR}$ of the area TH, obtained from AF demagnetisation (explanation, see Table 1)

Site	*N*/*M*	Geographic coordinates				Bedding	
		Dec.	Inc.	α_{95}	*k*	Dip dir.	Dip
mt1	5/10	**221.9**	**−20.6**	23.6	17.0	45.0	32.0
mt2	limited pyrrhotite content						
mt3	6/11	**22.4**	**24.5**	15.2	33.3	63.0	31.0
mt4	5/11	**329.8**	**57.5**	26.0	11.9	30.0	30.0
mt5	5/6	**24.7**	**25.4**	4.0	578.8	30.0	30.0
mt6	limited pyrrhotite content						
mt7	6/9	**349.3**	**35.9**	14.5	27.3	60.0	28.0
mt8	6/9	**194.9**	**−26.9**	12.1	31.8	65.0	33.0
mm9	7/10	345.4	−5.3	36.3	4.2	357.0–13.0	18.0–23.0
mm10	8/11	123.2	45.0	33.7	4.0	34.0	67.0
ms11	8/8	49.4	16.3	36.1	3.7	283.0	29.0
mt12	10/10	**7.1**	**30.9**	13.2	15.4	25.0	15.0
mt15	4/10	**358.5**	**28.2**	13.4	48.2	8.0	11.0
mt17	4/9	**12.4**	**30.7**	15.4	36.7	13.0	14.0
mt19	6/9	**327.3**	**41.3**	18.1	19.9	105.0	13.0
Mean 10 sites ($k > 10$)		Geographic coordinates					
		7.6	**34.0**	**13.4**	**13.9**		
		Stratigraphic coordinates					
		13.0	**15.3**	**15.6**	**10.5**		

^{39}Ar ages on muscovite from the Cambrian metasediments of Malari of 40.4 ± 1.1 Ma, which are interpreted as peak metamorphic ages representing the youngest thermal event in the TH area far from the STDS [31]. This age is consistent with the observed inclination of our remanence directions, coinciding with the expected ones from the APWP of India including a roughly estimated crustal shortening of 500 km (Fig. 6b).

In the LH area metamorphic temperatures were obviously higher. Illite crystallinity results from the Krol Belt area indicate anchizone–epizone transition grades, suggesting metamorphic temperatures of ~350°C [16], indicating a TRM mechanism for remanence acquisition. Also, the occurrence of antiparallel remanence directions in single samples both carried by pyrrhotite may indicate a thermal origin. A reversal record residing in a chemical remanence is unlikely because grain size variation would cause strong differences in the sequence of partial remanences unblocked during thermal demagnetisation compared to

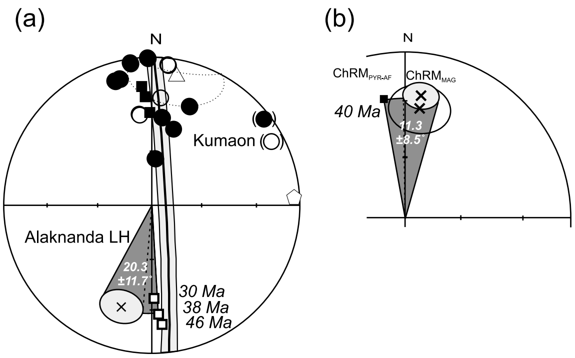

Fig. 6. (a) Determination of rotation of 20.3 ± 11.7° in the LH area by comparing the observed remanence direction (×; light grey area: α_{95} angle) with the APWP [26] for 38 Ma in the Alaknanda valley. For the Kumaon area results of forward modelling using least-squares fitting for a small-circle (black line; light grey area: α_{95} angle) fitted to the remanence directions of the pyrrhotite component including all sites except g5 and g21, marked in brackets. The pole (⬠) is plotted in the upper hemisphere. The apparent Fisher mean is represented by a triangle and its α_{95} angle by the dashed circle. Full/open squares show normal and reverse expected remanence direction. Dark grey area indicates the angle of rotation around vertical axes. (b) Determination of rotation of 11.3 ± 8.5° in the TH area by comparing the observed remanence direction with the APWP for 40 Ma for $ChRM_{MAG}$ and $ChRM_{PYR}$. See caption of Fig. 5b.

those acquired naturally [32,8]. The age of remanence acquisition of pyrrhotite can be related to the last cooling event through ~250–320°C [27,32]. ^{40}K/^{39}Ar cooling ages on illites of the Almora Group (Munsiari sheet, directly overlying the sampled formations) range from 11 to 39 Ma for the Alaknanda valley [16]. Older metamorphic ages for the Garhwal Lesser Himalaya may reflect older metamorphic events or may have been influenced by access argon or have been partly reset [16]. Radiometric ages for the southeastern part of the LH area are not available, but similar metamorphic conditions lead to the assumption of comparable ages.

5.2. Rotations north and south of the HHC

The accuracy of the result is dependent on the uncertainty of the pole determination and also on the model of reconstruction. In order to determine rotations with respect to the Indian plate the high-resolution (1 Ma) APWP of [26] (with α_{95} = 4.7°) is used. Nevertheless, using alternative APWPs of [33] and [34] (~10 Ma resolution) results in rotation larger by a few degrees and tens of degrees, respectively.

The small-circle distribution in the Kumaon LH area indicates a long-wavelength tilting over several tens of kilometers in the N–S direction after remanence acquisition. Such a late-orogenic tilting has also been observed in other areas of the Himalayas and cannot be unfolded by common bedding correction [11]. Duplex structures in the order of tens of kilometers north of the Dadeldhura synform and the Almora nappe, which have been formed between 12 and 5 Ma [15,21], may account for this tilting (Fig. 7). Deviation of the remanence directions by late-orogenic structures impedes age determination of the remanence acquisition when comparing the observed inclination to the APWP of India. No significant rotation results are obtained from this area (Fig. 6a).

In the Alaknanda valley later tilting after remanence acquisition is unlikely because of well-grouped remanence directions with a normal Gaussian distribution over a SW–NE profile of about 100 km. Therefore, the age of remanence acquisition of 38 ± 8 Ma (using [26]) can be deter-

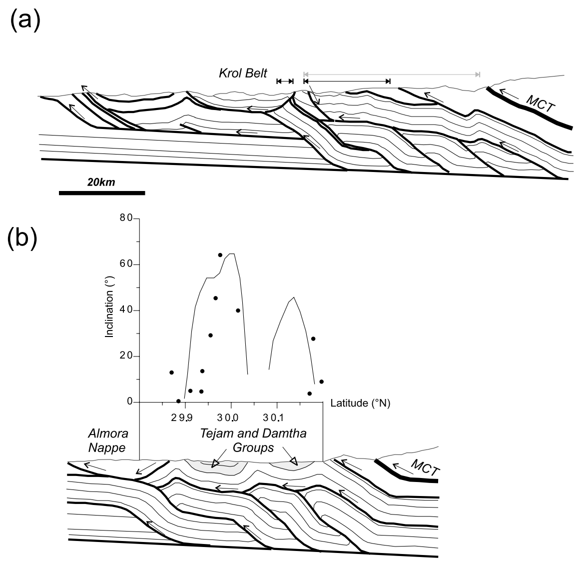

Fig. 7. Two structural profiles (not to scale) across the LH area in the NW and SE (simplified from [15]) show different duplex patterns. (a) The profile in the NW (Pr1 in Fig. 1b) shows a horizontal layer at the surface, which indicates no tilting caused by the duplex structure below. The black double arrows indicate the sites along the profile. The grey arrow indicates sites at comparable latitude, but samples W of the profile. (b) The profile in the SE (Pr2 in Fig. 1b) shows that the folding caused by the duplex structure is traced at the surface and the overlying horizontal layer is absent. This is consistent with the magnetic inclination pattern observed across this profile, as seen in the diagram. The black lines in the diagram represent the inverted dip of the duplex structure (stretched to the maximum inclination).

mined from the observed inclination if account is taken of a likely crustal shortening of about 200 km [17] along the thrusts to the south. This age is consistent with the cooling age of 39 Ma of [16]. This age has been ignored in the interpretation of [16].

A mean clockwise rotation of 20.3 ± 11.7° with respect to the Indian plate is resulting from the LH (Alaknanda valley) for a remanence age of 38 Ma. The uncertainties in ages lead to mean rotations of 18.1° for an age of 30 Ma and 22.6° for an age of 46 Ma.

In the TH area, the nearly identical directions of magnetite and pyrrhotite (Fig. 6b) suggest a comparable remanence acquisition age. Both components are of post-folding origin, as indicated by the negative fold test for the magnetite component and the secondary formation of pyrrhotite. Therefore, for the final interpretation, the better-defined magnetite component is used. For an age of 40 Ma a clockwise rotation of 11.3 ± 8.5° with respect to the Indian plate is obtained. The relatively small sampling area is not appropriate for identifying a possible overall tilting. However, the expected and observed inclinations for an age of 40 Ma are in good agreement and therefore late-orogenic tilting is unlikely.

The presented results show that significant clockwise rotations occurred north and south of the HHC since about 40 Ma. The approximately 10° difference in rotation between the Alaknanda valley and TH areas reveals no significant relative movement within uncertainty of overlapping α_{95} angles, but does not categorically exclude it.

6. Conclusions

This study provides palaeomagnetic data on a NE–SW transect across the MCT perpendicular to the strike of the Himalayan Arc. Our palaeomagnetic results are interpreted in terms of remanence acquisition ages, tilting and rotations with respect to the Indian plate and used for investigation of relative movements between the LH and TH.

In the southeastern Kumaon LH a late-orogenic shortening associated with the development of late stage tilting is concluded from the small-circle distribution of the remanence directions. This may be related to duplex structures north of the Almora nappe. The consistent inclination over about 100 km indicates a remanence acquisition age of 38 Ma in the Garhwal area. There is no evidence for tilting in the Garhwal and the TH area (or MCT ramping in the TH area) after 40–38 Ma. The different behaviour in tilting of the two areas traces the structural situation. Whereas in the Kumaon area the duplex structures caused long-wavelength folding at the surface, in the Garhwal area a relatively horizontal layer is outcropping at the surface [15] (Fig. 7). However, significant clockwise rotations occurred in both areas related to the rotational shortening, which includes the effects of both an overall rotation with respect to the Indian plate and oroclinal bending.

Comparable angles of rotation of LH and TH suggest that no relative rotational shortening due to counterclockwise rotation of India occurred along the MCT since 40 Ma. The apparently higher mean rotation angle of LH emphasises such an interpretation, although within α_{95} limits (upper boundary value for TH 19.8° clockwise, lower boundary value for LH 8.6° clockwise) the occurrence of such rotations cannot be rejected. Consequently, the more probable interpretation is that comparable angles of clockwise rotation of TH and LH indicate a common rotation of both units due to oroclinal bending along thrust(s) to the south of the MCT. The palaeomagnetic data of [4], interpreted in terms of rotational underthrusting of India along the MCT, leave open the possibility to locate underthrusting at large on more southern thrusts. The young age of the southern thrust (MBT, active since latest Miocene/Pliocene [21]) indicates that oroclinal bending is a young process, as already proposed by [34].

Acknowledgements

The German Research Council (DFG) funded this project. We would like to thank G. Fuchs for comments on regional geology. S.P. Singh kindly assisted the fieldwork. We would like to thank C.T. Klootwijk and two anonymous reviewers for constructive comments on an earlier draft of the manuscript. F. Martinez-Hernandez kindly commented on the results of the remanence anisotropy measurements.***[RV]***

References

[1] P.J. Treloar, M.P. Coward, Indian Plate motion and shape: constraints on the geometry of the Himalayan Orogen, Tectonophysics 191 (1991) 189–198.

[2] C.T. Klootwijk, P.J. Conaghan, C.McA. Powell, The Himalayan Arc: Large scale continental subduction, oroclinal bending and back-arc spreading, Earth Planet. Sci. Lett. 75 (1985) 167–183.

[3] A.R. Crawford, Narmada-Son lineament of India traced into Madagascar, J. Geol. Soc. India 19 (1978) 144–153.

[4] C. Klootwijk, D. Bingham, The extent of Greater India, 3. Palaeomagnetic data from the Tibetan Sedimentary Series, Thakkhola region, Nepal Himalaya, Earth Planet. Sci. Lett. 51 (1980) 381–405.

[5] E. Appel, R. Müller, R.W. Widder, Palaeomagnetic results from the Tibetan Sedimentary Series of the Manang area (north central Nepal), Geophys. J. Int. 104 (1991) 255–266.

[6] E. Appel, A. Patzelt, C. Chouker, Secondary palaeoremanence of Tethyan sediments from the Zanskar Range (NW Himalaya), Geophys. J. Int. 122 (1995) 227–242.

[7] E. Schill, E. Appel, O. Zeh, V.K. Singh, P. Gautam, Coupling of late-orogenic tectonics and secondary pyrrhotite remanences: Towards a separation of different rotation processes and quantification of rotational underthrusting in the western Himalaya (N-India), Tectonophysics 337 (2001) 1–21.

[8] C. Crouzet, H. Stang, E. Appel, E. Schill, P. Gautam, Detailed analysis of successive pTRMs carried by pyrrhotite in Himalayan metacarbonates: an example from Hidden Valley, Central Nepal, Geophys. J. Int. 146 (2001) 607–618.

[9] C.T. Klootwijk, A.K. Jain, K. Rakesh, Palaeomagnetic constraints on allochthony and age of the Krol Belt Sequence, Garhwal Himalaya, India, J. Geophys. 50 (1982) 127–136.

[10] E. Schill, E. Appel, P. Gautam, V.K. Singh, Preliminary palaeomagnetic results of the Lesser Himalaya, J. Nepal Geol. Soc. 18 (1998) 205–215.

[11] E. Schill, E. Appel, P. Gautam, Thermo-tectonic history of the Tethyan Himalayas deduced from palaeomagnetic record of metacarbonates from Central Nepal (Shiar Khola), J. Asian Earth Sci. 20 (2001) 203–210.

[12] P. Rochette, B. Scaillet, S. Guillot, P. LeFort, A. Pecher, Magnetic properties of the High Himalayan leucogranites: Structural implications, Earth Planet. Sci. Lett. 126 (1994) 217–234.

[13] A.K. Sinha, Geology of the Higher Central Himalaya, Intersci. Publ., 1989, 219 pp.

[14] K.S. Valdiya, Tectonics of the central sector of the Himalaya, in: H.K. Gupta, F.M. Delany (Eds.), Zagros, Hindu Kush, Himalaya, Geodynamic Evolution, Geodynamics Series 3, 1981, 323 pp.

[15] P. Srivastava, G. Mitra, Thrust geometries and deep structure of the outer and lesser Himalaya, Kumaon and Garhwal (India): Implications for evolution of the Himalayan fold-and-thrust belt, Tectonics 13 (1994) 89–109.

[16] G.J.H. Oliver, M.R.W. Johnson, A.E. Fallick, Age of metamorphism in the Lesser Himalaya and the Main Central Thrust zone, Garhwal India: results of illite crystallinity, 40Ar-39Ar fusion and K-Ar studies, Geol. Mag. 132 (1995) 139–149.

[17] K.V. Hodges, Overview: Tectonics of the Himalaya and

southern Tibet from two perspectives, Geol. Soc. Am. Bull. 3 (2000) 324–350.
[18] K.V. Hodges, D.S. Silverberg, Thermal evolution of the Greater Himalaya, Garhwal, India, Tectonics 73 (1988) 583–600.
[19] J.C. Vannay, K. Hodges, Tectonometamorphic evolution of the Himalayan metamorphic core between the Annapurna and Dhaulagiri, central Nepal, J. Metamorph. Geol. 14 (1996) 635–656.
[20] P.S. Saklani, Deformation and tectonism of Mukhem area, Lesser Himalaya, in: P.S. Saklani (Ed.), Tectonic Geology of the Himalaya. Current Trends in Geology, Today and Tomorrow's Printers and Publishers, New Delhi, 1978, pp. 15–42.
[21] P.G. DeCelles, D.M. Robinson, J. Quade, T.P. Ojha, C.N. Garzione, P. Copeland, B.N. Upreti, Stratigraphy, structure, and tectonic evolution of the Himalayan fold-thrust belt in western Nepal, Tectonics 20 (2001) 487–509.
[22] T. Ahmad, N. Harris, M. Bickle, H. Chapman, J. Bunbury, C. Price, Isotopic constraints on the structural relationships between the Lesser Himalayan Series and the High Himalayan Crystalline Series, Garhwal Himalaya, Geol. Soc. Am. Bull. 112 (2000) 467–477.
[23] F. Bergmüller, C. Bärlocher, B. Geyer, M. Grieder, F. Heller, P. Zweifel, A torque magnetometer for measurements of the high-field anisotropy of rocks and crystals, Meas. Sci. Technol. 5 (1994) 1466–1470.
[24] M. Waldhör, E. Appel, W. Frisch, A. Patzelt, Palaeomagnetic investigation in the Pamirs and its tectonic implications, J. Asian Earth Sci. 19 (2001) 429–451.
[25] P.L. McFadden, A new fold test for palaeomagnetic studies, Geophys. J. Int. 103 (1990) 163–169.
[26] G.D. Acton, Apparent polar wander of India since the Cretaceous with implications for regional tectonics and true polar wander, Mem. Geol. Soc. India 44 (1999) 129–175.
[27] R. Carpenter, Pyrrhotite isograd in Southeastern Tennessee and Southwestern North Carolina, Geol. Soc. Am. Bull. 85 (1974) 451–456.
[28] P. Rochette, Metamorphic control of the magnetic mineralogy of black shales in the Swiss Alps: toward the use of magnetic isogrades, Earth Planet. Sci. Lett. 84 (1987) 446–456.
[29] D.A. Crerar, N.J. Susak, M. Borcsik, S. Schwartz, Solubility of the buffer assemblage pyrite+pyrrhotite+magnetite in NaCl solutions from 200 to 350 degrees C, Geochim. Cosmochim. Acta 42 (1978) 1427–1438.
[30] I.B. Lambert, Post-depositional availability of sulphur and metals and formation of secondary textures and structures in stratiform sedimentary sulfide deposits, J. Geol. Soc. Aust. 20 (1973) 205–215.
[31] H. Williams, C. Prince, T. Argles, N.B.W. Harris, Thermal evolution of the Himalayan metamorphic belt, Garhwal, India: constraints from 40Ar-39Ar and Sm-Nd data, in: 16th HKTW Abstract volume, J. Asian Earth Sci. (2001) 75.
[32] C. Crouzet, G. Menard, P. Rochette, High-precision three-dimensional paleothermometry derived from paleomagnetic data in an alpine metamorphic unit, Geology 27 (1999) 503–506.
[33] J. Besse, V. Courtillot, Revised and synthetic apparent polar wander paths of the African, Eurasian, North American and Indian plates, and true polar wander since 200 Ma, J. Geophys. Res. 96 (1991) 4029–4050.
[34] C.T. Klootwijk, J.S. Gee, J.W. Peirce, G.M. Smith, Constraints on the India-Asia convergence: Paleomagnetic results from Ninetyeast Ridge, Proc. ODP Sci. Results 121 (1991) 777–882.